IEEE Access
Multidisciplinary | Rapid Review | Open Access Journal

Received June 14, 2020, accepted July 11, 2020, date of publication July 15, 2020, date of current version July 24, 2020.

Digital Object Identifier 10.1109/ACCESS.2020.3009433

Size Effect Study on High Frequency Transducers for Sensitivity Enhancement

ZHANGJIAN LI[1,2], (Member, IEEE), JIABING LV[1], XINLE ZHU[1], XIAOHUA JIAN[1], WEIWEI SHAO[1], (Member, IEEE), AND YAOYAO CUI[1], (Member, IEEE)

[1]Suzhou Institute of Biomedical Engineering and Technology, Chinese Academy of Sciences, Suzhou 215163, China
[2]University of Science and Technology of China, Hefei 230027, China

Corresponding author: Yaoyao Cui (cuiyy@sibet.ac.cn)

This work was supported in part by the National Natural Science Foundation of China under Grant 11704397, and in part by the National Key Research and Development Program of China under Grant 2018YFB2000200.

ABSTRACT In a high frequency ultrasonic imaging system, high signal-noise-ratio (SNR) is highly demanded to acquire high quality images. Transducer sensitivity enhancement is essential to increase the SNR. In this work, size effect of transducers with working frequency 12MHz and 20MHz is systematically studied to find its relationship with sensitivity. FEM (Finite Element Method) models are built to analyze the impedance and sound field characteristics for different size transducers. Pulse-echo measurement experiments are carried out to compare the performance variation induced by the size effect. Simulation results suggest that working frequency is mainly determined by the piezoelectric slice thickness, the values of admittance are dependent on the area value of transducers and the optimum width is 1.5mm-1.7mm for 12MHz transducer and 1.1mm-1.3mm for 20MHz transducer. The admittance measurement results and pulse-echo results confirm the simulation conclusion and certify that 12MHz transducer with 1.5mm width and 3.0mm length, 20MHz transducer with 1.2mm width and 3.0mm length have the highest sensitivities. Their echo peak-peak values can reach 1.248V and 1.332V, respectively. These results indicate that sensitivity can be enhanced by optimizing transducer size. Methods utilized in this work are of great significance in a broader range of transducer design cases such as IVUS system and array transducers.

INDEX TERMS FEM model, high frequency transducer, size effect, sensitivity enhancement.

I. INTRODUCTION

High frequency transducers are widely used in clinical applications such as intravascular ultrasound [1], ultrasound endoscopic [2] and ophthalmology [3]. Signal received from the high frequency transducer is usually weak since high frequency acoustic wave has high attenuation coefficient in tissue [4], fat, and muscle [5]. To obtain higher signal-noise-ratio (SNR) and improve image quality, it is essential to improve the sensitivity of high frequency transducer in ultrasonic imaging systems [6], [7].

The sensitivity of transducer is influenced by many factors including acoustic impedance matching [8], [9], electrical matching network [10], [11], cable transmission loss [12] etc. The acoustic impedance matching is realized by adding match layer between the resonant piezoelectric material and medium [13], matching layers are already indispensable for most of conventional medical transducers. RLC networks are adopted to reduce the electrical impedance mismatching [14]–[16]. This method is universal and is suitable for all kinds of transducers [11], [17]. However, the RLC network is of narrow bandwidth which is to be avoided in high frequency transducers [18]. To acquire broadband matching, complex multi-point matching RLC networks are needed [16]. The multi-point matching RLC networks increase the complexity of the image system, side effects such as frequency shifts off-resonance and overall system efficiency reduction cannot be ignored [19]. The cable transmission loss is inevitable because the transducer has to be wired to the system, so minimizing the cable length is necessary. An alternative method is interfacing an amplifier closely to the transducer before connecting to the cable, high sensitivity is achieved while additional noise was reduce and signal amplification was provided [20]. This method can isolate the cable effect, which has great influence on the performance of high frequency transducer [12]. Nevertheless, it becomes impossible to

The associate editor coordinating the review of this manuscript and approving it for publication was Ananya Sen Gupta.

integrate the amplifier to the transducers when transducers are too small in application scenario like ultrasonic bronchoscope.

Meanwhile, size effect of transducer on sensitivity is often neglected. KLM model presents equivalent circuits for transducers which several circuits are to be cascaded acoustically [21]. As the KLM model suggests, the size of transducer is closely related to its impedance characteristics [22]–[24]. The propagation theory of acoustic wave also proves that the receiving surface of transducer can directly affect the echo performance, while the receiving surface is also determined by the transducer size [25], [26]. This indicates that sensitivity enhancement can be achieved by optimization of the transducer size [27], [28].

In this work, we propose a method to increase the transducer sensitivity by optimizing transducer size. Theoretical analysis is firstly introduced to analyze the size effect. Then FEM models are built to simulate the impedance and sound field characteristics for different size transducers. Finally, verification experiments are carried out to compare the transducer performance change induced by the size effect through pulse-echo test. We pay attention on the sensitivity enhancement of single element transducer in this study. However, the technique can be used for any frequency range and it is not limited to transducer in this paper. The method can be easily expanded to other cases by simple modification.

II. MATERIALS AND METHODS

A. THEORETICAL ANALYSIS

The simplest transducer is a piece of piezoelectric plate with electrodes on the top and bottom as in Figure 1(a). The transducer can be described using the d-type piezoelectric equation in Equation (2.1).

$$\begin{cases} \mathbf{S} = s^E \mathbf{T} + d\mathbf{E} \\ \mathbf{D} = d\mathbf{T} + \varepsilon^T \mathbf{E} \end{cases} \tag{2.1}$$

Here, $\boldsymbol{E}$ is electric field, $\boldsymbol{T}$ is stress, $\boldsymbol{D}$ is electrical displacement and $\boldsymbol{S}$ is the strain. s^E is the elastic constant at short circuit, d is the piezoelectric strain coefficient, ε^T is the dielectric coefficient [29].

The impedance properties of a single piece of piezoelectric transducer can be represented near an isolated resonance by a lumped-parameter equivalent circuit in Figure 1(b) within its working frequency range, the parameters are approximately constant values [30].

R_1, L_1, C_0, and C_1 are the equivalent resistor, equivalent inductor, equivalent parallel capacitor, and equivalent series capacitor of transducer, respectively. Their element parameters can be descripted by Equation (2.2) to Equation (2.5).

$$R_1 = \frac{Z_\mathrm{m}}{4C_0^2 h^2} \tag{2.2}$$

$$L_1 = \frac{A\rho t}{8C_0^2 h^2} \tag{2.3}$$

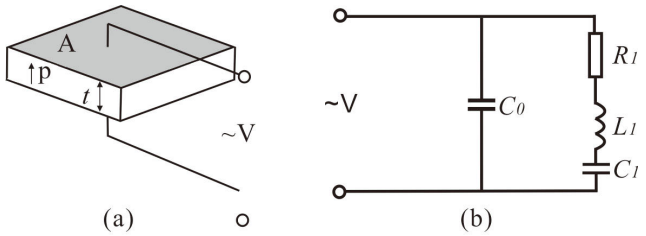

FIGURE 1. The RLC equivalent circuit.

$$C_1 = \frac{8C_0^2 h^2 t}{\pi^2 c^2 A\rho - 8C_0^2 h^2 t} \tag{2.4}$$

$$C_0 = \frac{\varepsilon A}{t} \tag{2.5}$$

Here Z_m is the radiation impedance of the material into which the transducer is radiating. In this work, Z_m is the electric impedance of matching layer [31]. t is the thickness of the piezoelectric plate, A is the area of the piezoelectric plate, ε is the permittivity without applied voltage, h is the piezoelectric pressure constant for the piezoelectric plate, ρ is the density.

As Equation (2.2), Equation (2.3), Equation (2.4), and Equation (2.5) indicate, the RLC parameters are highly related with the transducer size coefficient including thickness t and area A. For a rectangle plate, its area equals width multiplied by length. Thus, the impedance characters which directly affect the sensitivity of the transducer are determined by its thickness, width and length.

B. FEM SIMULATION MODEL

Since transducers with working frequencies of 12MHz and 20MHz are widely used in clinical application such as commercial ultrasound endoscopy. Enhancing the performance of these two kind of transducers is of great practical significance. In this work, transducers with working frequency 12MHz and 20MHz are researched. To simulate the characteristics of transducers, FEM models are built as shown in Figure 2 using COMSOL Multiphysics® (v.5.4. COMSOL AB, Stockholm, Sweden. 2018).

The acoustic impedance mismatching between piezoelectric material and transmission medium can cause ultrasound energy loss at the interface, resulting in poor sensitivity and long trailing wave [32]. The most common method to settle the mismatching is adding matching layer [13], [33]. Backing layer is employed to absorb the ultrasonic energy backward from the active piezoelectric layer and reduce the pulse durations [34]. Hence the transducer in our study has a sandwich construction which consist of backing layer, piezoelectric material layer and match layer.

The backing layer is made of epoxy with 85% Ag filled, it's Young's module is 50GPa, Poisson coefficient is 0.25, damping coefficient is 0.3, density is 3750 kg/m^3. The matching layer is home-made conductive glue mixture, its Young's module is 11GPa, Poisson coefficient is 0.3, damping coefficient is 0.2 and density is 1780kg/m^3. The mechanical

TABLE 1. Physical properties in the FEM models.

	Backing layer	Match layer	Piezo layer
Material	85wt% Ag filled epoxy	conductive glue mixture	PZT-5H
Thickness	500μm	12MHz:53μm 20MHz: 31μm	12MHz:165μm 20MHz: 95μm
Young's module	50GPa	11GPa	63GPa
Poisson coefficient	0.25	0.3	0.31
Mechanic damping	0.3	0.2	0.1
density	3750kg/m^3	1780kg/m^3	7500 kg/m^3

properties of the backing layer and matching layer are acquired by a standard testing procedure [35]. The piezoelectric material is PZT-5H, with Young's module 63GPa, Poisson coefficient 0.31, density 7500 kg/m^3. Its mechanical damping coefficient is calculated through its mechanical index Q, value is 0.1. For the 12MHz transducer, the thickness of piezoelectric material layer and match layer are 165um and 53um, respectively. And the thickness of piezoelectric material layer and match layer are 95μm and 31μm for the 20MHz [12]. The thickness parameters of backing layers are all 500μm for both transducers. The physical properties are shown in Table 1.

Considering the structural symmetry of length and width of transducers, a 2D simulation model is also established to simulate the sound pressure distribution along with the transducer steering direction. The physical properties is the same as Table 1. Water is set as the propagation medium, whose sound speed is 1500m/s and density 1000kg/m^3. The simulation model is shown in Figure 2(b).

Figure 2(a) is the 3D model, an actuate sine voltage with amplitude 100V is added on the upper and lower surface of piezoelectric layer. In order to simplify the model, control variables and highlight the influence of transducer size, free outer boundaries are selected in the model. Figure 2(b) is the 2D sound field model, it is actuated by the same actuate signal as Figure 2(a). Water is selected as the transmission medium. To simulate the infinite boundary, a non-reflecting boundary is added by setting its acoustic impedance as 1000kg/m^3 $\times$ 1500m/s [36]. A structure-acoustic boundary is set around the transducer to realize the transformation from transducer stress to sound field pressure. In Figure 2(b), model is meshed using free triangular method, maximum element size is set as 20μm in the water area and 50μm in the rest areas. On the premise of ensuring the accuracy of simulation, the meshing element size in Figure 2(a) is larger than that in Figure 2(b) to avoid out of memory. Free triangular method is used in the upper boundary, maximum element size is set as 40μm and then sweep to the whole 3D domain with maximum size 50μm. A voltage actuated signal is the same as the 3D model and added on the piezoelectric layer. The two models are both analyzed in frequency domain. For 12MHz transducer, frequency sweeps from 5MHz to 20MHz, step 0.5MHz.

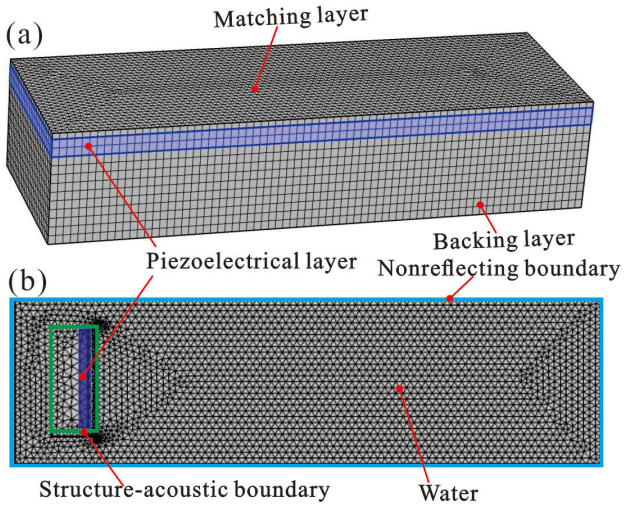

FIGURE 2. The simulation model, (a) 3D model, (b) 2D sound field model.

For 20MHz transducer, frequency sweeps from 10MHz to 35MHz, step 0.5MHz.

C. TRANSDUCERS FABRICATION AND PULSE-ECHO TEST

Transducers are fabricated according to the physical properties in Table 1. PZT-5H and matching layer slices are lapped to the desired thickness by precision grinding. Then Cr/Au electrodes with thickness of 100 nm are sputtered onto the upper and lower surfaces of PZT-5H slices. The PZT-5H slices with electrodes are then polarized under 3V/μm condition, i.e. 495V for 195μm and 285V for 95μm. PZT-5H layers and match layers are then bonded together using Epo-tek 301 (Epoxy Technology Inc., Billerica, MA), additional pressure is added to make sure that the glue layer is less than 1μm. The backing layer is mixed by epoxy and silver powder (wt% = 85%) and poured to the other Cr/Au electrode side of PZT-5H layer, then solidified at 60°, its thickness is controlled to 500μm through grinding. After that, the sandwich-layer devices are diced to the desired sizes through precision cutting. Before cable bonding, transducers are measured to obtain their electrical impedance curves on impedance analyzer (E4991A, Agilent Inc., CA, USA). Coaxial cables with length 30cm are bonded to the transducers using conductive silver epoxy H20S (Epoxy Technology Inc., Billerica, MA), the coaxial cables are 40AWG. Figure 3(a) is the sandwich structure of transducer samples with different sizes after dicing, and Figure 3(b) is the sample transducer with cable bonding.

To validate the simulation results, pulse-echo measurements are performed. The measurement setup is shown in Figure 4. Figure 4(a) is the schematic of measurement setup, it consists of water tank, position adjustment system, DPR 500 pulse generator/receiver, oscilloscope and acrylic plate. Transducers are immersed in water and temperature is kept as 20° during the measurement. The acrylic plate is the reflection target with thickness 5mm. Transducers are mounted on the position adjustment system to adjust its position and orientation to ensure the sound waves are

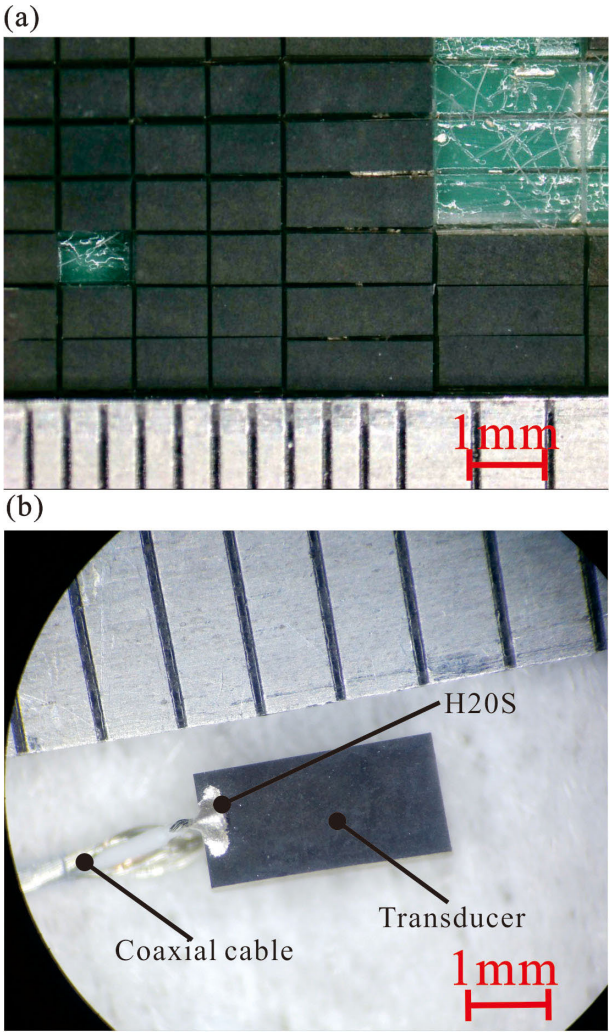

FIGURE 3. Samples, (a) after dicing, (b) after cable bonding.

incident perpendicular to the acrylic plate. The distance from the transducer to the acrylic plate is fixed as 10 mm so that the sound wave attenuation in the water is the same for all transducers with different sizes [37]. The transducers are actuated by the DPR 500 pulse Transmission/Receive system (Imaginant Inc., NY, USA), the actuated pulse was a unipolar negative pulse with the amplitude of 92.4 V and the FWHM pulse width of 3.2ns [12]. The receiving bandwidth and gain are set as 5-500 MHz and 0 dB, respectively. Received pulse signals are displayed and stored in the Tektronix DPO5034 oscilloscope (Tektronix, Inc., OR, USA), whose input impedance is set as 50Ω. Its digitalizing bit is 12 and corresponding quantification accuracy is 0.002V. To identify the small differences in sensitivity of different size of transducers, the significant digit of sensitivity results is chosen as 3.

III. RESULTS AND DISCUSSION

A. SIMULATION RESULTS

The admittance analysis is first conducted through the FEM model in Figure 2(a), the results are illustrated in Figure 5.

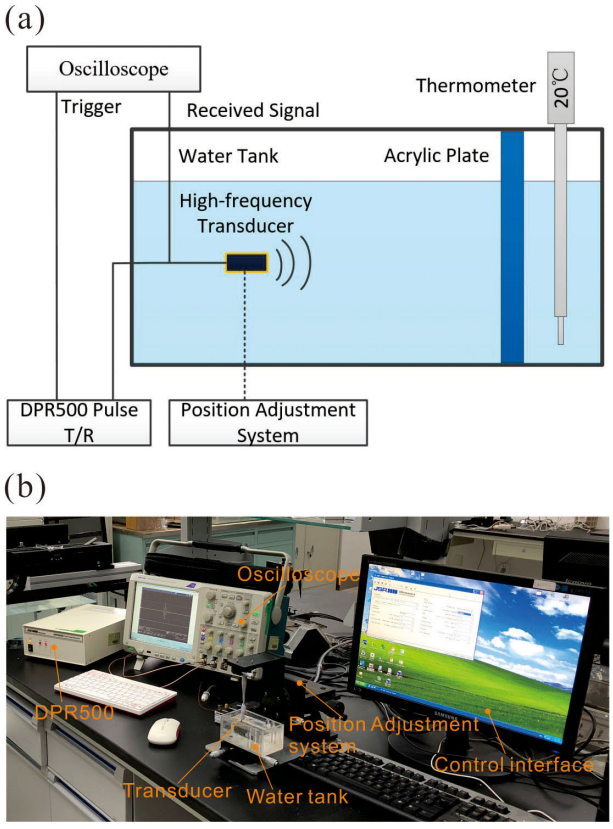

FIGURE 4. Pulse-echo measurement setup.

In the figure, each curve represents the relationship between admittance values of transducer and frequency.

Figure 5(a) is the simulation admittance curves of 12MHz transducer and Figure 5(b) is 20MHz. In Figure 5(a), the upper frequency f_h is about 15MHz, the lower frequency f_l is about 9MHz, the upper frequency and lower frequency determine the center frequency f_c which is nearly 12MHz. The locations of f_h, f_l and f_c are independent of the value of length and width. Values of admittance curve differ with the change of width and length. The curve with width 1mm, length 3mm coincides with the curve with width 1.5mm, length 2mm, they have the same area values. The admittance values differ from 2-3mS (width = 1mm, length = 2mm) to 12-27mS (width = 3mm, length = 3mm).

The results from 20MHz transducer model reflect the same change trend. In Figure 5(b), f_h, f_l and f_c are around 16MHz, 26MHz and 21MHz, respectively. Similar to the Figure 5(a), the curve with width 1mm, length 3mm is also coincides with the curve with width 1.5mm, length 2mm. The admittance values differ from 5-15mS (width = 1mm, length = 2mm) to 40-90mS (width = 3mm, length = 3mm).

The difference of f_h, f_l and f_c in (a) and (b) suggests that the working frequency is mainly determined by the piezoelectric plate thickness and not affected by its width and length. The values of admittance are dependent on the area value of transducers, the larger the area, the greater the admittance. For the same area value, admittance value of 20MHz transducer is bigger than 12MHz.

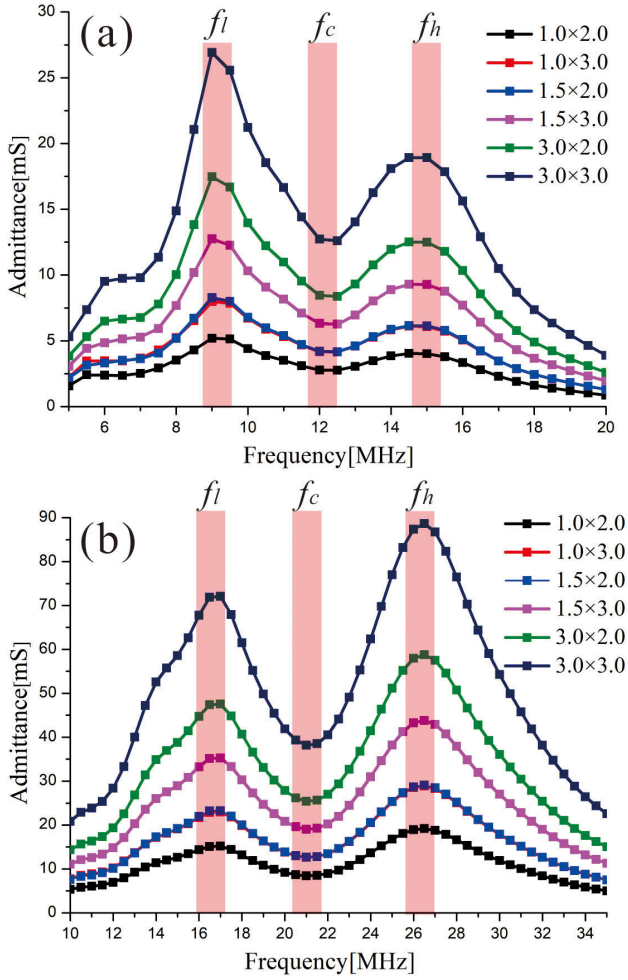

FIGURE 5. Simulation admittance curves, (a) 12MHz transducers, (b) 20MHz transducers.

Figure 6 is the sound field distribution along with the transducer steering direction at resonant frequency. Sound fields of different width transducers are listed. The width is 0.5mm, 1.0mm, 1.5mm, 2.0mm, 2.5mm and 3.0mm for both 12MHz and 20MHz transducer.

In Figure 6, two regions are clearly observed in all sound field results. The first region is the so-call near fields of transducers which is near the transducer face and displays interference between the face wave and edge wave. Their acoustic pressure distributions are disordered and unshaped. The second region locates at a distance away from the transducer and represents the transition to far-field behavior. The wave beams in the second region are narrower than those in the near field. The intensity distribution also shows uniform in the second region. These results in Figure 6 has high agreement with [36], [38]. This confirms the validity and accuracy of simulation model.

Figure 6(a) is the sound field of 12MHz transducers. It is obvious that the sound field intensity is very week when the width is 0.5mm, its near field is within the distance of 1mm. When the width increases to 1mm, the intensity is stronger but the distribution is disorder, its near field expands but within

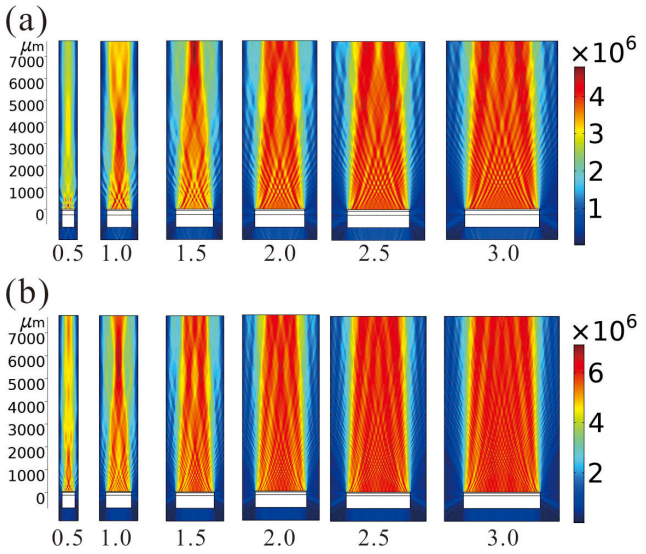

FIGURE 6. Sound field distribution, (a) 12MHz transducers, (b) 20MHz transducers.

the distance of 1.5mm. It becomes self-focus and with great intensity when width is 1.5mm, near field expands to within the distance of 2mm. The sound field intensity in 2.0mm, 2.5mm and 3mm are all considerable but distribution is dispersive compare to the situation of 1.5mm, their near field are all within the distance of 5mm.

Similarly, the results of 20MHz transducer display similar changing pattern in Figure 6(b). The sound field intensity is week and narrow without focusing when the width is 0.5mm. The sound field become intense, narrow, focusing and exhibits strong intensity when the width is 1.0mm. The sound field distributions in 1.5mm, 2.0mm, 2.5mm and 3mm are all dispersive with high intensity. The range of the near field increases with the width but all within the distance of 5mm

It is worth noting that the intensity of 20MHz is higher than 12MHz transducer when the width is equal.

As the results in Figure 6 indicate, the near fields of transducers are within the distance of 5mm. Since the disordered acoustical distribution in the near field of transducer cannot reflect the performance of transducer, the pressure values in a point which is away from the near field can be selected as the performance evaluation index.

Figure 7 shows the acoustic pressure values of different width transducers at the specific point. The distance between the point and transducer center is 7.5mm. In Figure 7(a), the pressure value reaches its maximum value when the transducer width is 1.5mm-1.7mm. In Figure 7(b), its maximum value is at 1.1mm-1.3mm. The results in Figure 7 suggest that the optimum width is 1.5mm-1.7mm for 12MHz transducer and 1.1mm-1.3mm for 20MHz transducer.

B. TRANSDUCER ADMITTANCE MEASUREMENT

Figure 8 is the electrical admittance curves of 12MHz transducers with different size without cable bonding from

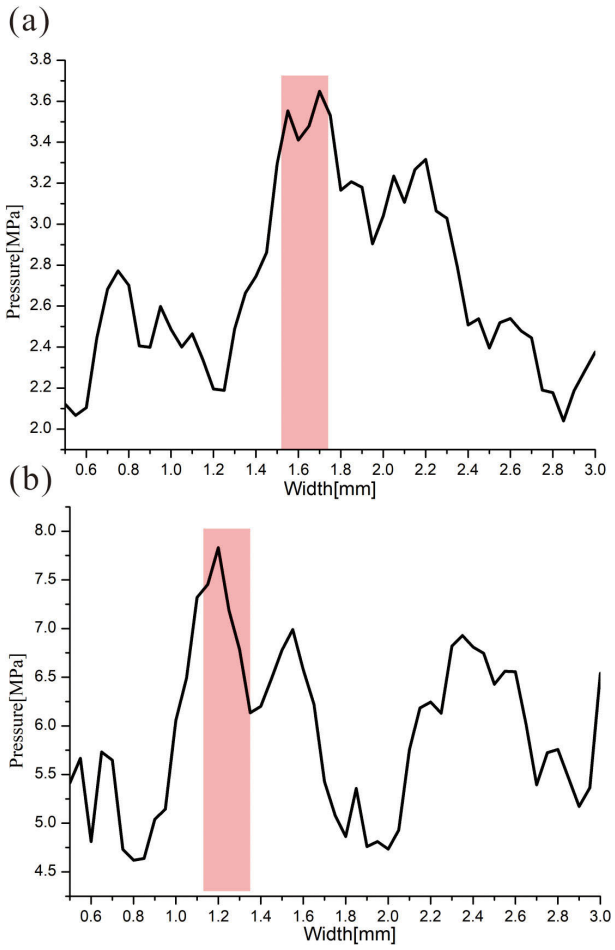

FIGURE 7. Sound pressure value at a distance of 7.5 mm, (a) 12MHz transducers, (b) 20MHz transducers.

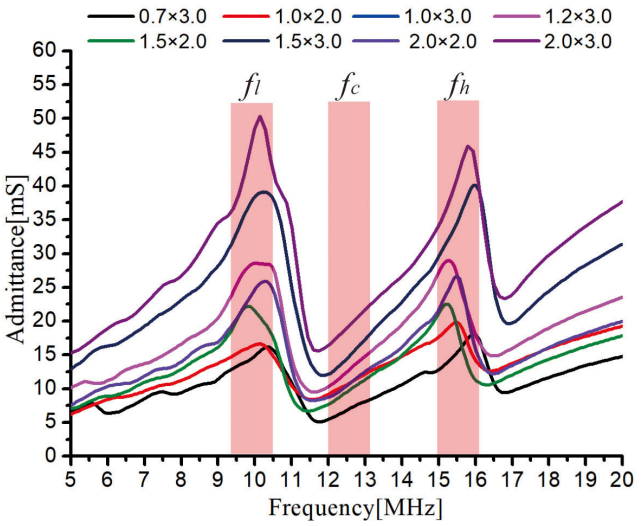

FIGURE 8. The impedance curve results of 12MHz transducers.

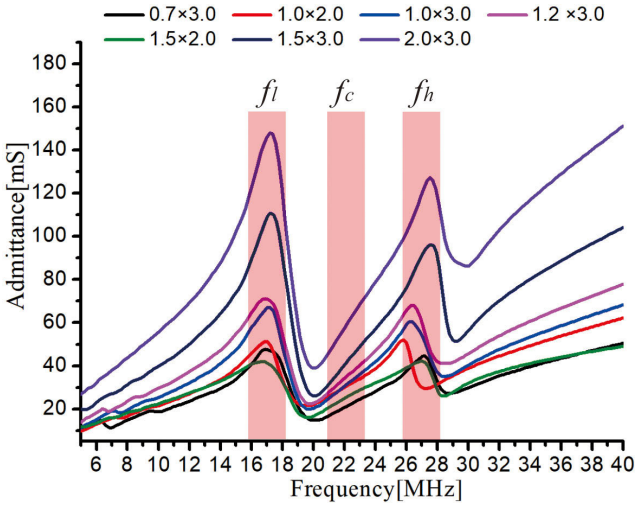

FIGURE 9. The impedance curve results of 20MHz transducers.

impedance analyzer (E4991A, Agilent Inc., CA, USA). The size of transducers are selected as: 0.7 × 3.0, 1.0 × 2.0, 1.0 × 3.0, 1.2 × 3.0, 1.5 × 2.0, 1.5 × 3.0, 2.0 × 2.0 and 2.0×3.0, all in millimeters. In Figure 8, the admittance curves have similar tendency to the simulation results in Figure 5(a), f_h, f_l and f_c are around 16MHz, 10MHz and 13MHz, which are slightly larger than that in Figure 5(a). The curves with equal areas (width = 1mm, length = 3mm and width = 1.5mm, length 2mm) have similar admittance values but not coincident. The admittance values are all bigger than that in Figure 5(a).

Similarly, Figure 9 is the electrical impedance curves of 20MHz transducers. The sizes of transducers are selected as: 0.7 × 3.0, 1.0 × 2.0, 1.0 × 3.0, 1.2 × 3.0, 1.5 × 2.0, 1.5 × 3.0 and 2.0 × 3.0. The admittance curves also have similar tendency to the simulation results in Figure 5(b), f_h, f_l and f_c are around17MHz, 27MHz and 22MHz, which are also slightly larger than that in Figure 5(b). The curves with equal areas (width = 1mm, length = 3mm and width = 1.5mm, length 2mm) have similar admittance values but difference is obvious. The admittance values are also bigger than that in Figure 5(b).

The admittance values in measurement are 5-50mS and 20-160mS for 12MHz and 20MHz, respectively. For the same size, the admittance values are larger than those in simulation. The curves are of different shapes. The values of f_h, f_l and f_c of simulation is slightly smaller. The reasons that cause the differences may include: boundary conditions, material parameters variation, epoxy glue layer lacking. The model in Figure 2(a) employ free boundary condition without any loading, while the transducers are clamped in the impedance analyzer during measurement. Material parameters in the simulation model are different from the actual situations. Epoxy glue layer may be another influence factor that cannot be ignored.

In spite of the differences between simulation and measurement, the conclusions from simulation results in Figure 5 still hold valid and are consistent with the experimental results. They are: the center frequency is mainly determined by the piezoelectric plate thickness. The values of admittance are

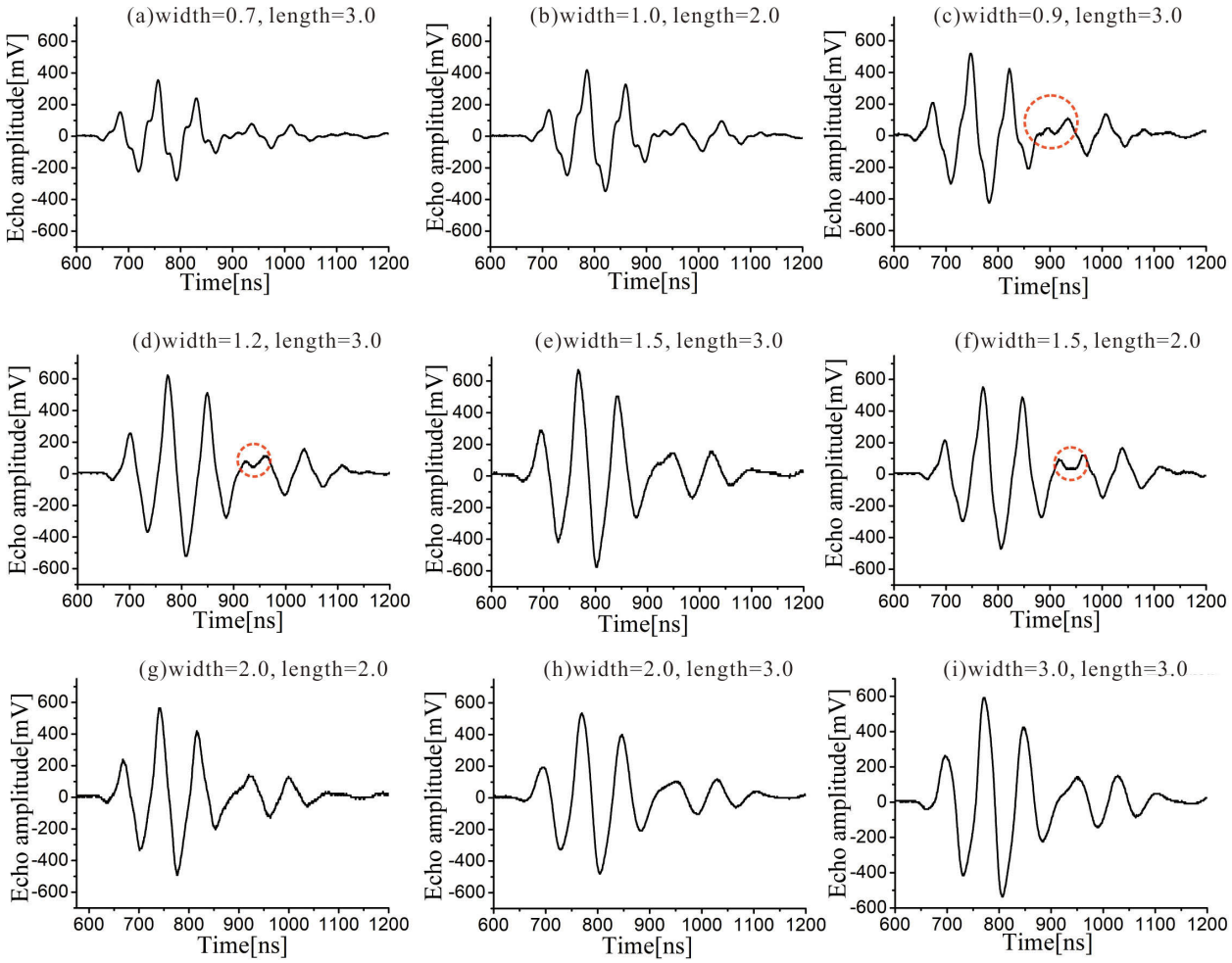

FIGURE 10. Pulse-echo results of different sizes 12MHz transducers.

dependent on the area value of transducers, the larger the area, the greater the admittance. For the same area value, admittance values of 20MHz transducer are bigger than 12MHz. This indicates that the simulation method in this manuscript can partly replace the experimental method and shorten the optimization process.

C. PULSE-ECHO RESULT

Transducer performances are evaluated by pulse-echo measurements. Figure 10 is the echo results of 12MHz transducers with different sizes. The sizes include: 0.7×3.0, 1.0×2.0, 0.9×3.0, 1.2×3.0, 1.5×2.0, 1.5×3.0, 2.0×2.0, 2.0×3.0 and 3.0×3.0, also in millimeters.

In Figure 10, obvious waveform distortions exist in (a), (b) and (c), such waveforms will cause image quality decline and not suitable for application [39]; in (d) and (f), waveform distortions still occur but comparable small; distortions are negligible in (e), (g), (h) and (i). The distortions may be related to the change of vibrator mode of the piezoelectric layer which is induced by the size change [40]. Their performance parameters including center frequency (f_c), -6dB pulse width (T_{06}), -6dB spectrum bandwidth (BW) and peak-to-peak value (V_{pp}) are list in Table 2.

In Table 2, center frequencies are all about 13MHz, value range is small. The value of T_{06} increases as the size, from 126.2ns (0.9×3.0) to 160.8ns (3.0×3.0).

The results of -6dB spectral bandwidth maintain between 44%-49%, displaying small value floating. The bandwidth is a very important evaluation index because broadband transducer improves resolution and image quality [41]. The bandwidth results in Table 2 are all near 50%, the difference among different size transducers is less than 6%. As the area increases, the bandwidth decreases slightly.

The values of V_{pp} are highly associated with the size parameters. The values are 636 mV, 768 mV and 844 mV for 0.7×3.0, 1.0×2.0 and 0.9×3.0 transducers. Their peak-to-peak values as well as sizes are smaller than others.

For 1.2×3.0, 1.5×2.0, 2.0×2.0, 2.0×3.0 and 3.0×3.0 transducers, their V_{pp} values are all over 1.0V. The 1.5×3.0 transducer has the highest sensitivity, its value is 1.248V. Its correspondent width locates at the interval which the simulation result in Figure 7(a) suggests.

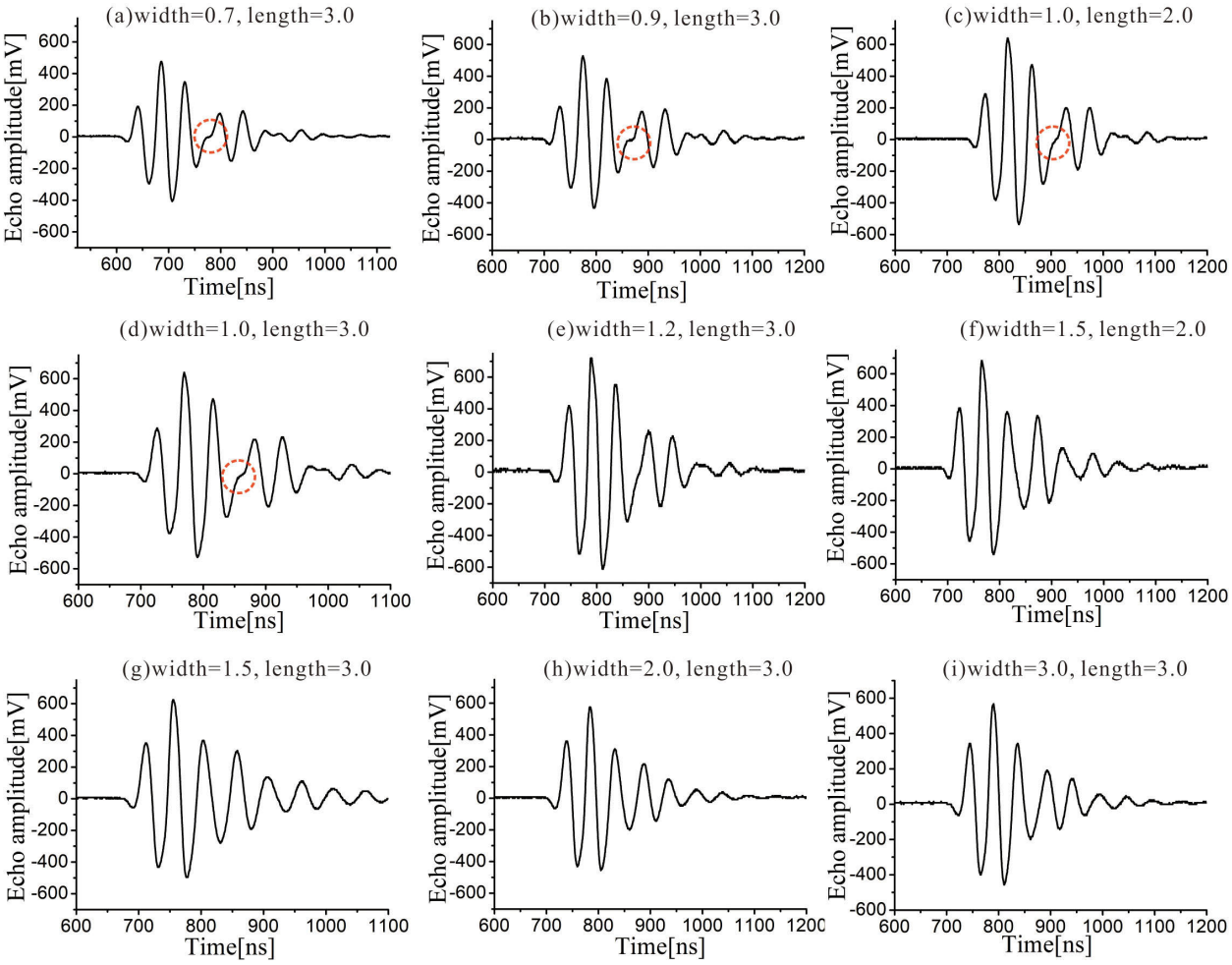

FIGURE 11. Pulse-echo results of different size 20MHz transducers.

TABLE 2. Performance parameters of 12MHz transducers.

Size(mm)	fc(MHz)	T06(ns)	BW(%)	Vpp(mV)
0.7×3.0	13.4	126.2	50.0	636
1.0×2.0	13.26	128.6	49.5	768
0.9×3.0	13.2	130.8	49.2	844
1.2×3.0	13.15	142	47.9	1144
1.5×2.0	12.85	140.4	49.0	1024
1.5×3.0	13.33	149.8	46.9	1248
2.0×2.0	13.13	137.2	48.4	1056
2.0×3.0	12.93	158.4	46.0	1016
3.0×3.0	13.23	160.8	44.2	1128

Figure 11 is the pulse-echo results of different size 20MHz transducers. The selected sizes are: 0.7 × 3.0, 0.9 × 3.0, 1.0 × 2.0, 1.0 × 3.0, 1.2 × 3.0, 1.5 × 2.0, 1.5 × 3.0, 2.0 × 3.0 and 3.0 × 3.0. As a whole, the waveforms of all echoes are roughly the same. The main difference is the small distortion and wave trailing. Waveform distortion exist in Figure 11(a), Figure 11(b), Figure 11(c) and Figure 11(d); in Figure 11(e), the distortions are minimum and disappear in Figure 11(f), Figure 11(g), Figure 11(h) and Figure 11(i). But the wave trailing in (f), (g), (h) and (i) is bigger than others. Their performance parameters are list in Table 3.

In Table 3, the values of center frequency are all about 21MHz, value range is small. The values of T_{06} stay within the range from 95ns to 105ns, all are less than 12MHz transducers. The −6dB spectral bandwidth maintains between 44%-48% for 0.7 × 3.0, 0.9 × 3.0, 1.0 × 2.0, 1.0 × 3.0, 1.2 × 3.0 transducers. The −6dB spectral bandwidth values of 1.5 × 2.0, 1.5 × 3.0, 2.0 × 3.0 and 3.0 × 3.0 decrease to nearly 30%, their waveforms also shows bigger wave trailing in Figure 11. The bandwidth decline induced by size change is greater than that of 12MHz transducers. This indicates that the bandwidth of 20MHz transducer is sensitive to the changes in area.

Similar to the 12MHz transducers, the values of V_{pp} in Table 3 are also highly dependent on the size parameters. The values are 844mV, 960mV for 0.7 × 3.0, 0.9 × 3.0 transducers, their values as well as sizes are smaller than others. 2.0 × 3.0, 3.0 × 3.0 transducers are of greater sensitivity, their peak-peak values are just over 1.0V, they have the biggest size areas.

TABLE 3. Performance parameters of 20MHz transducers.

Size(mm)	fc(MHz)	T_{06}(ns)	BW(%)	Vpp(mV)
0.7×3.0	21.9	96.2	47.5	884
0.9×3.0	21.83	95.8	47.9	960
1.0×2.0	21.85	100	47.1	1176
1.0×3.0	21.9	100.4	46.6	1168
1.2×3.0	21.9	109	43.8	1332
1.5×2.0	19.8	95.4	29.8	1224
1.5×3.0	20.35	102	26.5	1120
2.0×3.0	20.225	101.4	29.9	1032
3.0×3.0	20.5	104	30.7	1024

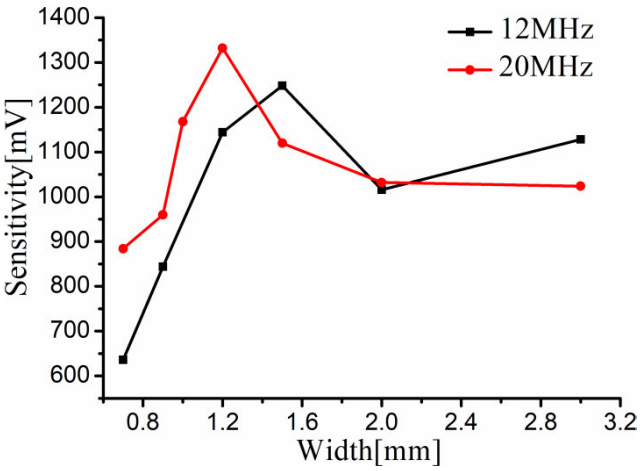

FIGURE 12. The relationship of sensitivity and transducer width.

For 1.0 × 2.0, 1.0 × 3.0, 1.2 × 3.0, 1.5 × 2.0, 1.5 × 3.0 transducers, their V_{pp} values are all over 1.1V. Among them, the 1.2 × 3.0 transducer has the highest sensitivity, its value reaches 1.332V. Its correspondent width is also near the optimum value in the simulation result of Figure 7(b).

Compared to the echoes of 12MHz transducers, the waveform distortions in Figure 11 are comparable small and show great consistency. Their sensitivity values are generally higher than those in Figure 10. And the values of - 6dB pulse width are also smaller. All those results agree well with the simulation results in Figure 6.

When transducer length is fixed as 3.0mm, the relationship between sensitivity and transducer width is illuminated in Figure 12. It is conspicuous that 12MHz transducer with 1.5mm width and 20MHz transducer with 1.2mm width have the highest sensitivity. For the transducers in this study, their sensitivities are very dependent on the width when the width is less than 2.0mm. When the width is over 2.0mm, the changing trend becomes moderated.

When transducer length is fixed as 2.0mm, 12MHz transducers with size 1.0 × 2.0, 1.5 × 2.0 and 2.0 × 2.0 have echo amplitude 768mV, 1024mV and 1056mV, all weaker than 1.5 × 3.0 transducer. 20MHz transducers with size 1.0 × 2.0 and 1.5 × 2.0 have echo amplitude 1176mV and 1224mV, also weaker than 1.2 × 3.0 transducer. If the transducer length and width continue to decrease, it is easy to infer that there will be signal distortion and sensitivity decline in the echoes according to the results in Figure 10, Figure 11 and Table 2, Table 3.

Therefore, 12MHz transducer with 1.5mm width, 3.0mm length and 20MHz transducer with 1.2mm width, 3.0mm length are of the optimal size, in which the highest sensitivity will be achieved.

In above discussion, the sensitivity analysis is performed based on the 10 mm distance from the transducers. Since the attenuation in medium is a basic characteristic of sound wave, which is independent of transducer size [37], [42], the conclusions and optimized geometries hold for other distances.

In this work, the sensitivity of single element transducers is studied. It is worth noticing that this technique can be used for any frequency range and is not limited to single element transducers. After simple modifications, the simulation model and analysis method utilized in this work can be easily expanded to a broader range of transducer design cases such as multi-element transducers, focused transducers, and other aspects. The required modifications include the changing of boundary condition, transducer shape, polarization direction etc.

However, the method in this study will encounter some new problems when analyzing other parameters which is related with wave propagation, transducer vibration characteristics etc. For example, the crosstalk analysis between elements in array transducer is not available. More effort is needed to address these deficiencies in the future researches.

IV. CONCLUSION

In this research, size effect of transducers is studied to enhance sensitivity. Simulation results suggest that working frequency is mainly determined by the piezoelectric plate thickness and not affected by its width and length. The values of admittance are dependent on the area value of transducers, and the optimum width is 1.5mm-1.7mm for 12MHz transducer and 1.1mm-1.3mm for 20MHz transducer. The pulse-echo results confirm that 12MHz transducer with 1.5mm width, 3.0mm length and 20MHz transducer with 1.2mm width, 3.0mm length have the highest sensitivity. Their echo amplitudes can reach 1.248V and 1.332V respectively. These results indicate that the simulation models in this work can be applied to speed up transducer design, the sensitivity can be enhanced by optimizing transducer size. This method will provide new design idea for high frequency transducer and be of great significance in the application such as ultrasound endoscopic, IVUS system, and array transducers.

ACKNOWLEDGMENT

The authors thank the helpful comments from the reviewers. The authors also would like to thank Miss Ang Li from Suzhou Guoke Ultra Medical Technology Co., Ltd., for helping transducers cable bonding. Suzhou Guoke Ultra Medical Technology Co., Ltd. also provided measurement conditions.

REFERENCES

[1] T. Ma, M. Yu, Z. Chen, C. Fei, K. Shung, and Q. Zhou, "Multi-frequency intravascular ultrasound (IVUS) imaging," *IEEE Trans. Ultrason., Ferroelectr., Freq. Control*, vol. 62, no. 1, pp. 97–107, Jan. 2015, doi: 10.1109/TUFFC.2014.006679.

[2] B. D. Lindsey, J. Kim, P. A. Dayton, and X. Jiang, "Dual-frequency piezoelectric endoscopic transducer for imaging vascular invasion in pancreatic cancer," *IEEE Trans. Ultrason., Ferroelectr., Freq. Control*, vol. 64, no. 7, pp. 1078–1086, Jul. 2017, doi: 10.1109/TUFFC.2017.2702010.
[3] R. Silverman, "Focused ultrasound in ophthalmology," *Clin. Ophthalmol.*, vol. 10, pp. 1865–1875, Sep. 2016, doi: 10.2147/opth.s99535.
[4] K. K. Shung, "High frequency ultrasonic imaging," *J. Med. Ultrasound*, vol. 17, no. 1, pp. 25–30, 2009, doi: 10.1016/S0929-6441(09)60012-6.
[5] D. W. Park, D. C. Park, and S. H. Chung, "Ultrasound signal processing technique for subcutaneous-fat and muscle thicknesses measurements," *IEEE Access*, vol. 7, pp. 155203–155208, 2019, doi: 10.1109/ACCESS.2019.2949073.
[6] J.-F. Chen and D.-C. Liu, "Ultrasound imaging system and method," *J. Acoust. Soc. Amer.*, vol. 113, no. 5, p. 2398, 2003, doi: 10.1121/1.1584199.
[7] C.-W. Wei, T.-M. Nguyen, J. Xia, B. Arnal, E. Y. Wong, I. M. Pelivanov, and M. O'Donnell, "Real-time integrated photoacoustic and ultrasound (PAUS) imaging system to guide interventional procedures: *Ex vivo* study," *IEEE Trans. Ultrason., Ferroelectr., Freq. Control*, vol. 62, no. 2, pp. 319–328, Feb. 2015, doi: 10.1109/tuffc.2014.006728.
[8] C. Fei, J. Ma, C. T. Chiu, J. A. Williams, W. Fong, Z. Chen, B. Zhu, R. Xiong, J. Shi, T. K. Hsiai, K. K. Shung, and Q. Zhou, "Design of matching layers for high-frequency ultrasonic transducers," *Appl. Phys. Lett.*, vol. 107, no. 12, Sep. 2015, Art. no. 123505, doi: 10.1063/1.4931703.
[9] S. Gupta, G. Haiat, C. Laporte, and P. Belanger, "Effect of acoustic impedance mismatch between skin and bone on transcranial ultrasound transmission," *J. Acoust. Soc. Amer.*, vol. 144, p. 1747, Oct. 2018, doi: 10.1121/1.5067746.
[10] G. Kim, M.-K. Seo, N. Choi, K. S. Baek, and K.-B. Kim, "Application of KLM model for an ultrasonic through-transmission method," *Int. J. Precis. Eng. Manuf.*, vol. 20, no. 3, pp. 383–393, Mar. 2019, doi: 10.1007/s12541-019-00050-y.
[11] Y. Yang, X. Wei, L. Zhang, and W. Yao, "The effect of electrical impedance matching on the electromechanical characteristics of sandwiched piezoelectric ultrasonic transducers," *Sensors*, vol. 17, no. 12, p. 2832, Dec. 2017.
[12] X. Jian, Z. Li, Z. Han, J. Xu, P. Liu, Y. Liu, Y. Cui, and W. Huang, "The study of cable effect on high-frequency ultrasound transducer performance," *IEEE Sensors J.*, vol. 18, no. 13, pp. 5265–5271, Jul. 2018, doi: 10.1109/JSEN.2018.2838142.
[13] Q. Zhou, J. Cha, Y. Huang, R. Zhang, W. Cao, and K. K. Shung, "Alumina/epoxy nanocomposite matching layers for high-frequency ultrasound transducer application," *IEEE Trans. Ultrason., Ferroelectr., Freq. Control*, vol. 56, no. 1, pp. 213–219, Jan. 2009, doi: 10.1109/tuffc.2009.1021.
[14] S. Lin, "Radiation impedance and equivalent circuit for piezoelectric ultrasonic composite transducers of vibrational mode-conversion," *IEEE Trans. Ultrason., Ferroelectr., Freq. Control*, vol. 59, no. 1, pp. 139–149, Jan. 2012.
[15] S. Lin and J. Xu, "Effect of the matching circuit on the electromechanical characteristics of sandwiched piezoelectric transducers," *Sensors*, vol. 17, no. 2, p. 329, Feb. 2017.
[16] J. An, K. Song, S. Zhang, J. Yang, and P. Cao, "Design of a broadband electrical impedance matching network for piezoelectric ultrasound transducers based on a genetic algorithm," *Sensors*, vol. 14, no. 4, pp. 6828–6843, Apr. 2014.
[17] J. Zhang, Z. Long, C. Wang, F. Ren, and Y. Li, "Novel optimization approach in ultrasonic machining: Unilateral compensation for resonant vibration in primary side," *IEEE Access*, vol. 7, pp. 34131–34140, 2019, doi: 10.1109/access.2019.2895960.
[18] H. Huang and D. Paramo, "Broadband electrical impedance matching for piezoelectric ultrasound transducers," *IEEE Trans. Ultrason., Ferroelectr., Freq. Control*, vol. 58, no. 12, pp. 2699–2707, Dec. 2011.
[19] O. J. Norman, G. Hilton, and M. Beach, "Measurement of efficiency degradation due to external detuning of a tunable patch antenna," in *Proc. IEEE Int. Symp. Antennas Propag. (APSURSI)*, Jun./Jul. 2016, pp. 2145–2146.
[20] C. Yang, X. Jian, X. Zhu, J. Lv, Y. Jiao, Z. Han, A. Stylogiannis, V. Ntziachristos, G. Sergiadis, and Y. Cui, "Sensitivity enhanced photoacoustic imaging using a high-frequency PZT transducer with an integrated front-end amplifier," *Sensors*, vol. 20, no. 3, p. 766, Jan. 2020, doi: 10.3390/s20030766.
[21] R. Krimholtz, D. A. Leedom, and G. L. Matthaei, "New equivalent circuits for elementary piezoelectric transducers," *Electron. Lett.*, vol. 6, no. 13, pp. 398–399, 1970, doi: 10.1049/el:19700280.
[22] A. Ballato, "Modeling piezoelectric and piezomagnetic devices and structures via equivalent networks," *IEEE Trans. Ultrason., Ferroelectr., Freq. Control*, vol. 48, no. 5, pp. 1189–1240, Sep. 2001.
[23] Z. Jin, L. Huo, T. Long, X. Guo, J. Tu, and D. Zhang, "An online impedance analysis and matching system for ultrasonic transducers," *IEEE Trans. Ultrason., Ferroelectr., Freq. Control*, vol. 66, no. 3, pp. 591–599, Mar. 2019, doi: 10.1109/TUFFC.2018.2889073.
[24] P. Maréchal, F. Levassort, L.-P. Tran-Huu-Hue, and M. Lethiecq, "Lens-focused transducer modeling using an extended KLM model," *Ultrasonics*, vol. 46, pp. 67–155, May 2007, doi: 10.1016/j.ultras.2007.01.006.
[25] J. A. Jensen and N. B. Svendsen, "Calculation of pressure fields from arbitrarily shaped, apodized, and excited ultrasound transducers," *IEEE Trans. Ultrason., Ferroelectr., Freq. Control*, vol. 39, no. 2, pp. 262–267, Mar. 1992, doi: 10.1109/58.139123.
[26] A. Alia, "Ultrasonic diffraction by a circular transducer: Isogeometric analysis sensitivity to full gauss quadrature points," *J. Acoust. Soc. Amer.*, vol. 147, no. 2, pp. EL74–EL79, Feb. 2020, doi: 10.1121/10.0000591.
[27] X. Li, D. Lyu, Y. Song, S. Zhang, P. Hu, and H. Jeong, "Simultaneously determining sensitivity and effective geometrical parameters of ultrasonic piezoelectric transducers using a self-reciprocity method," *IEEE Trans. Ultrason., Ferroelectr., Freq. Control*, vol. 66, no. 10, pp. 1649–1657, Oct. 2019, doi: 10.1109/TUFFC.2019.2925834.
[28] S. Sarangapani and X. Yan, "Improvement in the electromechanical properties of a partially diced piezoelectric disc transducer," *IEEE Access*, vol. 6, pp. 70324–70330, 2018, doi: 10.1109/ACCESS.2018.2879463.
[29] W. G. Cady, "Piezoelectric equations of state and their application to thickness-vibration transducers," *J. Acoust. Soc. Amer.*, vol. 22, no. 5, pp. 579–583, Sep. 1950, doi: 10.1121/1.1906654.
[30] *IEEE Standard on Piezoelectricity*, ANSI/IEEE Standard 176-1987, 1988, p. 0_1, doi: 10.1109/IEEESTD.1988.79638.
[31] C. S. Desilets, J. D. Fraser, and G. S. Kino, "The design of efficient broadband piezoelectric transducers," *IEEE Trans. Sonics Ultrason.*, vol. 25, no. 3, pp. 115–125, May 1978, doi: 10.1109/T-SU.1978.31001.
[32] H.-S. Hsu, F. Zheng, Y. Li, C. Lee, Q. Zhou, and K. Shung, "Focused high frequency needle transducer for ultrasonic imaging and trapping," *Appl. Phys. Lett.*, vol. 101, Jul. 2012, Art. no. 24105, doi: 10.1063/1.4736731.
[33] F. Guo, Y. Wang, Z. Huang, W. Qiu, Z. Zhang, Z. Wang, J. Dong, B. Yang, and W. Cao, "Magnesium alloy matching layer for PMN-PT single crystal transducer applications," *IEEE Trans. Ultrason., Ferroelectr., Freq. Control*, vol. 65, no. 10, pp. 1865–1872, Oct. 2018, doi: 10.1109/TUFFC.2018.2861394.
[34] T. Kondo, "Carbon-fiber composite materials for medical transducers," in *Piezoelectric and Acoustic Materials for Transducer Applications*, A. Safari and E. K. Akdoğan, Eds. Boston, MA, USA: Springer, 2008, pp. 179–188.
[35] S. Allameh, B. Gally, S. B. Brown, and W. Soboyejo, *Mechanical Properties of Structural Films*. West Conshohocken, PA, USA: American Society for Testing and Materials, 2001.
[36] J. Cheeke and J. Zagzebski, "Fundamentals and applications of ultrasonic waves," *Amer. J. Phys.*, vol. 72, p. 719, Apr. 2004, doi: 10.1119/1.1645288.
[37] D. Xiao, Q. Fan, C. Xu, and X. Zhang, "Measurement methods of ultrasonic transducer sensitivity," *Ultrasonics*, vol. 68, pp. 150–154, May 2016, doi: 10.1016/j.ultras.2016.02.017.
[38] J. E. Soneson, "Ultrasound propagation in tissue," in *Theory and Applications of Heat Transfer in Humans*, Devashish Shrivastava. Burnsville, MN, USA: Wiley, 2018, pp. 167–182.
[39] S. J. Huang, "Ultrasound physics," in *Echocardiography in ICU*, M. Slama, Ed. Cham, Switzerland: Springer, 2020, pp. 1–23.
[40] D. A. Berlincourt, D. R. Curran, and H. Jaffe, "Piezoelectric and piezomagnetic materials and their function in transducers," in *Physical Acoustics: Principles and Methods*, vol. 1, A. Warren and P. Mason, Eds. New York, NY, USA: Academic, 1964, doi: 10.1016/B978-1-4832-2857-0.50009-5.
[41] R. H. Silverman, E. Vinarsky, S. M. Woods, F. L. Lizzi, and D. J. Coleman, "The effect of transducer bandwidth on ultrasonic image characteristics," *Retina*, vol. 15, no. 1, pp. 37–42, 1995, doi: 10.1097/00006982-199515010-00008.
[42] A. L. Lopez-Sanchez and L. W. Schmerr, "Determination of an ultrasonic transducer's sensitivity and impedance in a pulse-echo setup," *IEEE Trans. Ultrason., Ferroelectr., Freq. Control*, vol. 53, no. 11, pp. 2101–2112, Nov. 2006, doi: 10.1109/TUFFC.2006.150.

ZHANGJIAN LI (Member, IEEE) received the B.S. degree in instrument science and technology from the University of Science and Technology of China, Hefei, China, in 2011, and the master's degree in optical engineering from the University of Chinese Academy of Sciences, Beijing, China, in 2014. He is currently pursuing the Ph.D. degree with the University of Science and Technology of China. He is currently an Associate Researcher with the Medical Ultrasound Department, Suzhou Institute of Biomedical Engineering and Technology, Chinese Academy of Sciences, Suzhou, Jiangsu, China. His research interests include micro medical ultrasound transducer and its applications.

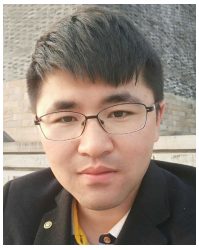

JIABING LV received the B.S. and master's degrees in microelectronic technology from Soochow University, Suzhou, China, in 2014 and 2017, respectively. He is currently an Assistant Researcher with the Medical Ultrasound Department, Suzhou Institute of Biomedical Engineering and Technology, Chinese Academy of Sciences. His research interests include ultrasonic array design and fabricate technology.

XINLE ZHU received the B.S. and master's degrees in mechanical manufacturing and automation from the Nanjing University of Aeronautics and Astronautics, Nanjing, China, in 2014 and 2017, respectively. He is currently an Assistant Researcher with the Medical Ultrasound Department, Suzhou Institute of Biomedical Engineering and Technology, Chinese Academy of Sciences. His research interests include ultrasonic array design and fabricate technology.

XIAOHUA JIAN received the B.S. degree in optics information science and technology and the Ph.D. degree in physics from Xi'an Jiaotong University, China, in 2005 and 2011, respectively. In 2011, he joined the Suzhou Institute of Biomedical Engineering and Technology, Chinese Academy of Sciences, as a Research Assistant, where he was promoted to a Researcher, in 2017. His research interests include ultrasonic transducer design and fabrication, photoacoustic imaging, and optics spectroscopy.

WEIWEI SHAO (Member, IEEE) received the Ph.D. degree from the Department of Precision Machinery and Precision Instrumentation (PMPI), University of Science and Technology of China. She is currently a Professor with the Medical Ultrasound Department, Suzhou Institute of Biomedical Engineering and Technology, Suzhou, China. Her research interests include piezoelectric transformer, and high-frequency piezoelectric transducer and its application.

YAOYAO CUI (Member, IEEE) received the M.S. and Ph.D. degrees in biomedical engineering from Xi'an Jiaotong University, China, in 1999 and 2002, respectively. She has worked as a Postdoctoral Researcher with CREATIS, INSA de Lyon, in 2003, and was appointed by the Medical Vision Laboratory, University of Oxford, as a Postdoctoral Research Associate, in 2004. In 2007, she held a position as a Research Fellow with the University of Dundee. Since 2011, she joined the Suzhou Institute of Biomedical Engineering and Technology (SIBET), CAS, China, as a Hundred Talents Professor. She was the Director of the Medical Imaging Department. She is also the Director of the Medical Ultrasound Department. Her research interests include ultrasound imaging, ultrasound bio-effects, and photoacoustic.